2003

An experimental and theoretical study of transient negative ions in Mg, Zn, Cd and Hg

J. P. Sullivan

Paul Burrow

D. S. Newman

K. Bartschat

J. A. Michejda

See next page for additional authors

Authors

J. P. Sullivan, Paul Burrow, D. S. Newman, K. Bartschat, J. A. Michejda, P. Panajotovic, M. Moghbelalhossein, R. P. McEachran, and Stephen J. Busckman

New Journal of Physics
The open access journal at the forefront of physics

Deutsche Physikalische Gesellschaft DPG IOP Institute of Physics

OPEN ACCESS

An experimental and theoretical study of transient negative ions in Mg, Zn, Cd and Hg

New Journal of Physics
An Institute of Physics and Deutsche Physikalische Gesellschaft Journal

An experimental and theoretical study of transient negative ions in Mg, Zn, Cd and Hg

J P Sullivan[1], P D Burrow[2], D S Newman[1], K Bartschat[3], J A Michejda[2], R Panajotovic[1], M Moghbelalhossein[1], R P McEachran[1] and S J Buckman[1,4]

[1] Atomic and Molecular Physics Laboratories, Research School of Physical Sciences and Engineering, Australian National University, Canberra, ACT, Australia

[2] Department of Physics and Astronomy, University of Nebraska, Lincoln, NE, USA

[3] Physics Department, Drake University, Des Moines, IA, USA

E-mail: stephen.buckman@anu.edu.au

New Journal of Physics **5** (2003) 159.1–159.26 (http://www.njp.org/)
Received 30 September 2003
Published 9 December 2003

Abstract. A range of experimental and theoretical techniques have been applied to the study of transient negative ions (resonances) formed in electron scattering from the Group II metals Mg, Zn, Cd, and Hg at incident electron energies below the first ionization potential. A wealth of resonance structures have been observed and from the experimental observations and theoretical information, classifications are proposed for some of these negative ion states.

[4] Author to whom any correspondence should be addressed.

Contents

1. Introduction

Temporary negative ions, or resonances, are a common occurrence in low-energy electron–atom (molecule) scattering spectra. These states form as a result of the projectile electron of a well-defined energy being bound for a short period of time to the atom or molecule which can also be excited during the collision process. The lifetimes of these states are typically in the range 10^{-14}–10^{-12} s and, as such, investigations in their own temporal domain are difficult. However, in many cases, they can have a profound effect on electron scattering cross-sections and they are usually studied by measurements of the energy dependence of such scattering cross-sections (excitation functions) where the character of the electron involved in the decay (autodetachment) of the resonance can often be identified. Although these excited states are ubiquitous in atomic and molecular physics, their detailed study has been confined to a rather restricted range of atomic targets, principally the rare-gas atoms and one-electron systems such as hydrogen and the alkalis. A review of studies up until the early part of the last decade is contained in [1].

In their work on the Group II atoms, Burrow *et al* [2] noted that the full outer ns^2 subshell means that they do not readily form stable negative ions. However, because their lowest unfilled np and nd orbitals have the same principal quantum number as the highest filled orbitals, the 'additional' ($l > 1$) electron lies at rather low energies and feels a strong influence of the polarization and centrifugal potentials which are known to lead to the formation of shape resonances. Much of the early work on these atoms focused on the existence of the lowest-lying ns^2np shape resonances and these have been observed, for instance, in the electron transmission studies of Burrow *et al* [2, 3] and Johnston and Burrow [4]. Interestingly, no such resonance was observed in Ca and the late 1980s has seen an interesting sequence of events leading to the observation of a bound state of Ca^- [5]–[7].

Although there is a reasonably substantial body of experimental work on higher-lying resonances in the two-electron Group II atoms, particularly Hg, most of this work consists of measurements which are equivalent to integral cross-sections and there are only a few studies which provide unambiguous information on the classifications of the observed resonances. In Mg, the only previous studies which seriously treat the presence of resonances are the electron transmission spectroscopy (ETS) measurements of Burrow and Comer [3] and Burrow *et al* [2] and the optical excitation functions of Shpenik *et al* [8]. For Zn, the situation is similar with only the optical excitation function measurements of Shpenik *et al* [9] and the ETS measurements of Burrow *et al* [2] in the literature. In Cd, there are several excitation function measurements [9, 10], the ETS measurements of Burrow *et al* [2], the spin-polarized electron scattering measurements of Bartsch *et al* [11] and the elastic scattering data of Panajotovic *et al* [12]. There are also recent measurements by Kontros *et al* [13, 14] of elastic scattering, total scattering, the ionization yield and excitation of the $5s5p\,^{3,1}P$ states. In the above cases, where resonances are observed and discussed, this discussion is generally restricted to those features that have been observed at relatively low energies, up to and including the thresholds for the $nsnp\,^{3,1}P$ excited states in these atoms ($n = 3, 4, 5, 6$ respectively for Mg, Zn, Cd and Hg). Mercury appears to be the exception as, perhaps due to the relative ease of producing an atomic mercury beam, there is a substantial body of work on higher-lying resonances and several attempts have been made at classifications for the wealth of structures that have been observed. It is not appropriate to catalogue all of the previous Hg studies here and the interested reader can find a reasonably comprehensive account of these in [1]. However, there is a still a substantial body of work which is of relevance to the present investigation, in particular the early work of Heddle [15, 16], Albert *et al* [17], Koch *et al* [18], Newman *et al* [19] Hanne *et al* [20] and references therein. The work of Newman *et al* is perhaps the most comprehensive of all, offering energies, classifications and widths of a large number of resonances observed in the metastable atom excitation function. Of contemporary interest, and in some sense a precursor to this paper, is a recent letter by Burrow *et al* [21], which discusses the classification of resonances near the $6s6p\,^3P_{0,1,2}$ excited states of Hg.

Theoretical interest in negative ion states in the Group II atoms has also been reasonably strong, although mostly aimed at the study of the lowest energy ns^2np shape resonance. These calculations, for each of the Group II atoms, have been summarized in [1].

In the present work we have combined experimental information from a range of scattering measurements together with theoretical *R*-matrix (RM) calculations. The experimental techniques include (i) electron transmission measurements (ETS), conducted at the University of Nebraska, on Mg, Zn, Cd and Hg, (ii) elastic differential scattering measurements conducted at the Australian National University (ANU) on Mg, Zn and Cd and (iii) optical excitation functions for the lowest excited states of Mg and Cd, also carried out at the ANU. As we hope to demonstrate, this provides for a powerful combination of one technique, which is extremely sensitive to the presence of sharp resonances (ETS) and another, which provides information on the angular momentum carried away by the autodetached electron (angular differential scattering). In addition, we have also studied these resonances in a number of optical excitation functions for excited states of the neutral atom which give further information regarding the likely resonance configurations. These experimental studies are supported by calculations using the RM method which provides detailed information on the eigenphases involved in resonant scattering from Mg, Cd and Hg. We concentrate,

in the present work, on resonances which have been observed near the thresholds of the $nsnp\,^{3,1}P$ excited states of these atoms but some speculative observations are made on higher-lying states. Some aspects of this work on Mg and Cd have been published previously [22].

2. Experimental considerations

An experimental approach which has been extensively used for resonance studies is ETS [23]. In these experiments, a resonance structure appearing in the total scattering cross-section is detected with high sensitivity by measuring directly the derivative, with respect to energy, of the electron current transmitted through a vapour cell containing the gas of interest. The derivative technique serves to greatly enhance any sharp resonance structure with respect to the slowly varying background. This technique has been used in the present experimental studies at the University of Nebraska to study resonances in Mg, Zn, Cd and Hg. The electron source is a trochoidal monochromator with an energy resolution of approximately 35–50 meV. A standard gas cell was wrapped with insulated tungsten wire to provide resistive heating. Separate heaters were used on the gas cell and the reservoir containing the solid metal to be vaporized. The absolute energy scale is set by observing the large and well-studied shape resonances in the 2 eV region when N_2 is admitted into the experimental chamber along with the metal vapour beam. The estimated uncertainty in the electron beam energy for these experiments is ± 30 meV.

The above techniques provide accurate and extremely sensitive information about the energy and width of resonance structures and their role in the total scattering cross-section. However, the scattered electrons are not detected and they therefore do not provide information about the nature of the autodetached electron from which the resonance configuration can be obtained. There are distinct advantages associated with resonance measurements that include the detection of the energy and angle of the electron that is autodetached in the decay of the resonant state. In many cases, this provides information about the final neutral atomic state involved in the decay and also the angular momentum that the scattered electron carries with it. Such information can then be used, together with simple arguments based on angular momentum and parity conservation, and the nature of the entrance channel, to deduce the symmetry of the resonant state.

Such an apparatus, which employs crossed electron and atomic beams, has been used for the experiments at the ANU. This apparatus employs an hemispherical energy selector in tandem with electrostatic electron optics to produce a high-resolution electron beam (30–35 meV) which is crossed with a metal vapour beam effusing from a resistively heated oven. The oven consists of two sections, a reservoir chamber with a volume of $\sim 100\,cm^3$ which is linked via a small tube to an hypodermic needle having 1 mm diameter and 10 mm length which serves as the oven exit. The reservoir and the needle are independently heated using coaxial bifilar heating elements and the exit needle is kept approximately 50 °C hotter than the reservoir. The oven reservoir is located in a differentially pumped 'source' chamber and the tube and needle protrude into the 'scattering' chamber which contains the electron spectrometer. The tip of the needle lies about 5 mm below the electron beam axis and the effusing atomic beam crosses the electron beam to form the interaction region which is at the centre of the scattering chamber.

A range of detectors, including two retarding potential analysers (RPA), a photomultiplier and a metastable atom detector are used to measure the energy dependence of a range of reaction products—elastic electrons, decay photons and metastable atoms—that arise from the electron collision. The two retarding potential analysers consist of a simple arrangement of grids and a channeltron detector (Dr Sjuts model KBL5RS). They are mounted on a small turntable and they rotate in a plane which contains the incident electron beam and is orthogonal to the atomic beam—the traditional scattering plane. In this way, scattering angles between 25° and 120° can be accessed and measurements of elastic scattering at two angles can be achieved simultaneously. A photomultiplier, mounted in a re-entrant vacuum feedthrough, also views the interaction volume via a series of lenses and an interference filter which selects the wavelength of interest. Excitation functions for elastic scattering or the yield of decay photons are measured under computer control. The computer steps the incident electron energy and the signals from the three detectors are stored in a multichannel analyser as is the digitized electron beam current, measured with a Faraday cup. In the present series of measurements two photomultipliers have been used. The first is a solar blind tube (Thorn EMI model 9405) which was used for measurements of UV (< 300 nm) lines and the second (Thorn EMI model 9131 Q/100) for measurements in the visible region. This second tube also had a small (3 mm diameter) photocathode to reduce dark noise. A number of techniques have been used to calibrate the incident energy in these measurements. Initially, it was done by using elastic scattering in N_2 and using the positions of the quasi-vibrational peaks in the $^2\Pi$ resonance near 2 eV [24]. However, for most of the measurements, the well-known energies [25] for the thresholds of decay photon production for either the $nsnp\,^3P$ or ^1P states has been used. The estimated uncertainty in the energy scale is again ± 30 meV.

3. Numerical calculations

The calculations performed for this work are similar to those described in detail by Scott *et al* [26] for the mercury target. Briefly, we performed RM (close coupling) calculations including the $ns^2\,^1S$ and $nsnp\,^{3,1}P$ states with $n = 3$ (Mg), $n = 4$ (Zn), $n = 5$ (Cd) and $n = 6$ (Hg) in the close coupling plus correlation expansion of the $(N + 1)$-electron system consisting of the projectile electron and the N-electron target. For e–Mg collisions, we also performed a larger calculation including the states of the configurations 3s4s, 3s4p and 3s3d, respectively. Relativistic effects were accounted for through the one-electron spin–orbit term in describing the e–Cd and e–Hg collision processes, while non-relativistic models were used for e–Mg and e–Zn. The non-relativistic models will be labelled by 'LS3' or 'LS9' and the relativistic models will be labelled 'BP5' below, with the digit indicating the number of coupled states. The one-electron bound-orbital bases were generated with the structure programs CIV3 of Hibbert [27] for the Mg and Zn targets and with SUPERSTRUCTURE of Eissner *et al* [28] for Cd and Hg. Configuration mixing with $np^2\,^1S$ was always included to improve the description of the ground state. Finally, instead of performing an all-electron calculation for e–Hg scattering, a model potential was applied to represent the effect of the 78 inner electrons.

The semi-relativistic RM code of Berrington *et al* [29] was employed to perform the inner-region calculation with appropriately chosen box sizes between 25 and 40 Bohr radii to ensure that exchange effects between the projectile and the target electrons could be neglected outside the RM sphere. The use of 25 continuum basis orbitals for each orbital angular momentum

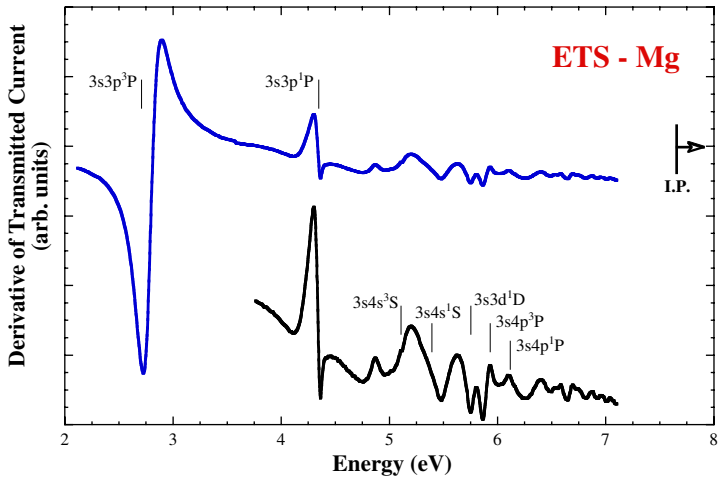

Figure 1. The derivative of the transmitted electron current for magnesium as a function of incident electron energy. The positions of a number of neutral excited states are indicated by the vertical bars. The lower curve is merely an expanded section of the upper curve.

of the projectile was sufficient to represent its motion inside the sphere, and summing the contributions from orbital angular momenta up to 15 yielded convergence of the partial-wave expansion for all energies of interest for the present work. The calculation for the external region was performed using the flexible asymptotic RM package FARM of Burke and Noble [30].

Although state-of-the-art computer architecture might suggest that much bigger calculations should be performed to describe the collisions studied experimentally in the present work, we opted for the simpler models for several reasons. To begin with, the BP5 calculations of Scott *et al* [26] for e–Hg collisions were quite successful (see also the recent paper by Herting *et al* [31]). Furthermore, including additional channel coupling effects, for example, through target states of the configuration $ns(n+1)p\,^{3,1}P$, can actually become problematic. As one might expect from atomic-structure theory, including such states by providing an additional p-orbital has little effect on the quality of the description for the lower target states. However, it can strongly affect the position of the $nsnp^2$ negative-ion resonances, usually pushing them too low with respect to the corresponding thresholds in the neutral. Unfortunately, driving the close-coupling expansion effectively to convergence is very difficult for these systems, particularly since opening up of the outermost closed d-shell seems to be required. Further efforts in this direction are currently in progress, but their description goes beyond the scope of the present work.

4. Experimental results

4.1. Magnesium

Although magnesium has the same ns^2 outer electron configuration as all the atoms we consider here, it differs from all others in that its d-shell is empty. The electron transmission spectrum for magnesium, in the energy region between 2 and 7 eV is shown in figure 1. Many

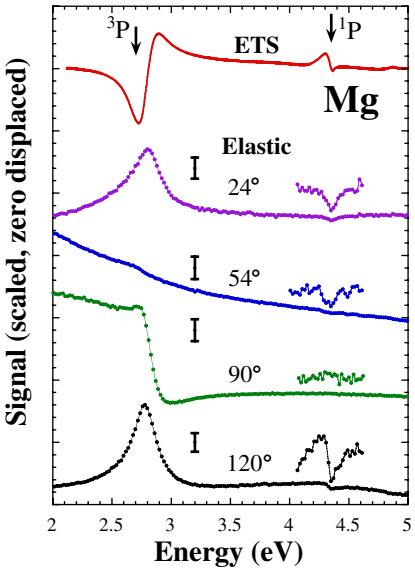

Figure 2. The derivative of the transmitted electron current (top), and the differential elastic scattering signal for magnesium as a function of energy in the vicinity of the 3s3p excited state thresholds. For the elastic scattering data the zeros have been displaced and the vertical bars represent approximately 20% of the scattered intensity.

resonance features are evident and in many cases there is an apparent correspondence between the occurrence of a resonance and the threshold for a neutral excited state, some of which are indicated by vertical bars. One striking exception to this is the feature at 4.87 eV which lies well below the 3s4s ^{3}S threshold. The ETS data in the energy region between 2 and 4.5 eV, in the neighbourhood of the 3s3p ^{3,1}P excited state threshold, are highlighted in figure 2, together with the complementary data from the elastic scattering experiments at scattering angles of 24, 54, 90 and 120°. Also indicated in this figure are the thresholds for the 3s3p $^3P_{0,1,2}$ and $^1P_1$ neutral excited states. Two large resonance features are clearly visible in the ETS spectra near the excited state thresholds. The feature near the $^3P_{0,1,2}$ thresholds, which occur at 2.709, 2.712 and 2.717 eV respectively, also appears in the elastic scattering spectrum, although not at all scattering angles—it is present at 24, 90 and 120° but not at 54°. The striking aspect about the elastic scattering spectra is the dominant nature of this resonance contribution, indicated by the vertical bars on the spectra which represent approximately 20% of the total scattering intensity at each angle. This is particularly the case at scattering angles of 90 and 120° and, at 90° for instance, the steep drop in the excitation function represents a change in the elastic scattering cross-section across the resonance of about 80%. A strong resonance is also apparent in the ET spectrum at around 4.30 eV, near the threshold of the 3s3p $^1P_1$ excited state which occurs at an energy of 4.346 eV [25]. As we shall see in the following sections, this difference between the resonance energy and the excited state energy (∼20–30 meV) is larger in Mg than the corresponding feature in all of the other atoms studied here. This resonance is also visible in the elastic scattering spectra at all of the scattering angles studied, although to do so it must be highlighted through background subtraction and zero suppression.

Magnesium is a well-LS-coupled atom and therefore, unlike some of the heavier Group II atoms, the 3s3p $^3P_1$ state has a very low transition probability. As a result photons

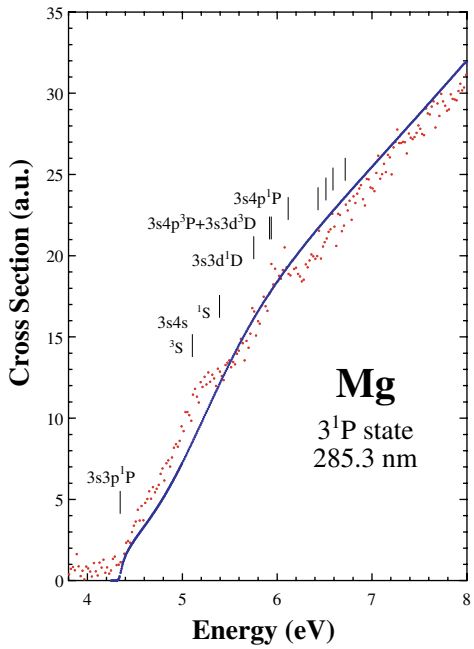

Figure 3. Optical excitation function for the 3s3p ^{1}P state of magnesium between threshold and 8 eV. The solid line is the 3-state RM calculation to which the experimental data have been normalized at an energy of 6 eV. The vertical bars indicate the energies of excited state thresholds, some of which are labelled. The vertical scale is in atomic units (a.u.).

arising from the decay of this state to the ground state could not be observed. However, the 3s3p $^1P_1$ state radiates at a wavelength of 285.3 nm and the excitation function for this state is shown in figure 3. Here we have normalized the experimental data to the 3-state RM calculations at an energy of 6 eV. Although the counting statistics are poor the excitation function is relatively featureless. However, there is a sharp step at threshold and background subtraction reveals two broad structures at around 5.2 and 6.0–6.2 eV. There is good overall agreement between experiment and theory regarding the energy dependence of the cross-section and the calculation indicates that the cross-section is quite large.

In figure 4 we show a comparison of the experimental elastic scattering data with the RM predictions at each scattering angle. In each case, the theoretical cross-section curve has been convoluted with a Gaussian instrumental function of 40 meV FWHM and the experimental data have been normalized to the calculation at an energy of 2 eV. At more forward angles (24°, 54°) both the direct scattering cross-section and the resonant contribution are very large and at all angles, except 54°, the resonant contribution to the cross-section is greater than 50%. At each angle, the general features of the measured excitation function are well reproduced by the calculation, although there are some differences which may be due, in part, to background contributions in the experimental data. The agreement between experiment and theory regarding the precipitous drop of the elastic cross-section at 90° as it passes through the resonance region is particularly impressive. At each angle the main resonance feature appears at a slightly lower energy in the calculation, although the position of the resonance near the 3s3p $^1P_1$ threshold is in good accord with the experiment at each angle.

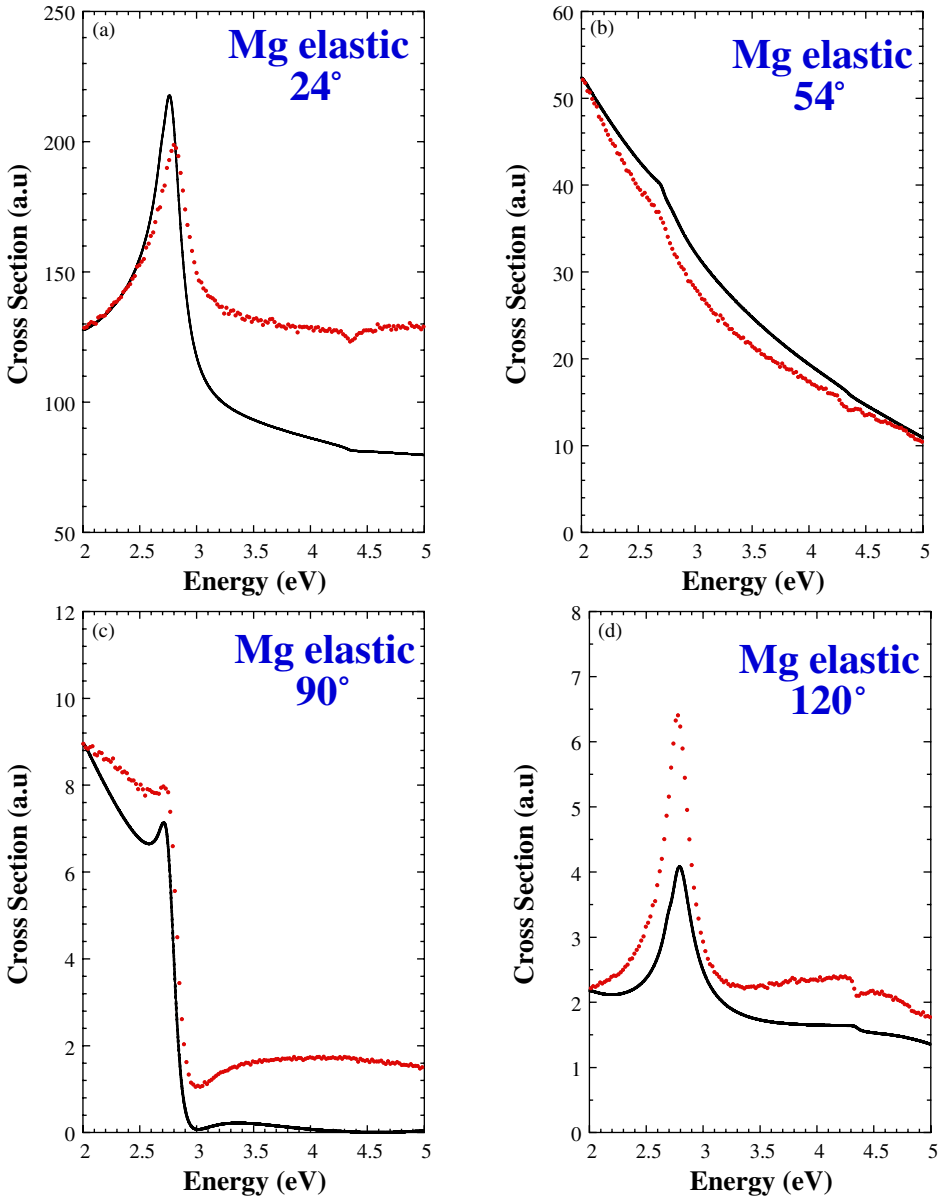

Figure 4. Comparison of experiment and theory (solid line) for elastic electron scattering from Mg at (a) 24°, (b) 54°, (c) 90° and (d) 120°. In each case, the experiment has been normalized to the theory at an energy of 2 eV. The vertical scale is in atomic units (a.u.).

4.2. Zinc

The ETS spectrum for zinc is shown in figure 5. The spectrum below the $^2S_{1/2}$ ionization potential is similar to that for Mg with many resonances observed. In the case of Zn however, the ETS spectrum also extends above the ionization potential and a further series of strong resonances is observed, presumably associated with zinc autoionizing levels. Also, in figure 4, we show the positions of a number of neutral excited states of Zn and once again see a correlation between the energies of these states and the resonance energies. Note that the

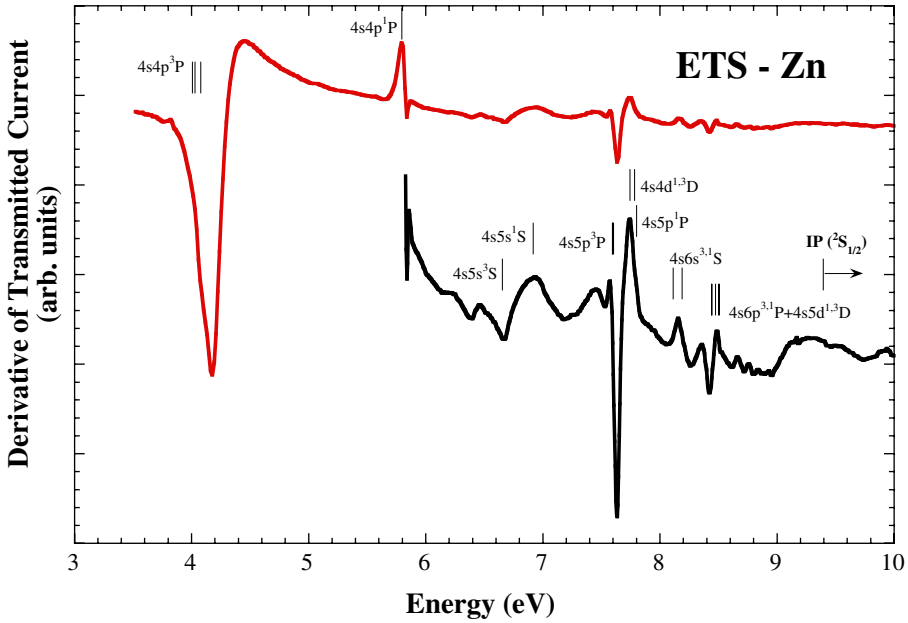

Figure 5. The derivative of the transmitted electron current for zinc as a function of incident electron energy. The positions of a number of neutral excited states are indicated by the vertical bars. The lower curve is merely an expanded section of the upper.

larger (∼70 meV) separation of the three states in the 4s4p ^{3}P manifold in Zn, compared with that of the 3s3p ^{3}P in Mg (5 meV), is indicative of the increased spin–orbit interaction in Zn. One, and possibly two, resonances are seen near the 4s4p ^{3}P thresholds. One of these is the largest feature in the ETS spectrum and the other is a small bump located well below the excited state thresholds, at approximately 3.81 eV. A further, strong feature is located within a few meV of the threshold of the 4s4p ^{1}P state (compare with Mg where the corresponding feature was some 40 meV below the 3s3p ^{1}P state) and two further resonances appear at energies below the next neutral excited level, the 4s5s ^{3}S state. A broad feature is observed to overlap the 4s5s ^{3,1}S thresholds whilst near the 4s5p ^{3}P thresholds two narrow features are evident, one much stronger than the other, and they have a shape which is similar to the features at the 4s4p ^{3}P threshold. A similar, but somewhat more compressed and considerably weaker sequence of features is again observed near the energies of the 4s6s and 4s6p thresholds. There are obviously many additional features leading up to the ionization limit at 9.39 eV, but these, and the nearby neutral excited states, are highly overlapping. A broad bump precedes the ionization potential and there is apparently a 'step' in the derivative spectrum just above the IP.

In figure 6 we highlight the ETS spectrum in the region near the 4s4p ^{3,1}P thresholds and include data from elastic scattering studies, albeit at a limited range of angles. The situation in zinc is very similar to that observed in magnesium with a dominant, broad and strong resonance near the threshold for the 4s4p ^{3}P$_{0,1,2}$ states (which occur at energies 4.006, 4.030 and 4.078 eV, respectively) and a further structure at or near the ^{1}P threshold (which occurs at 5.796 eV). There is also a hint in figures 5 and 6 of a further, weak structure below the ^{3}P thresholds at an energy of about 3.81 eV. Where comparison can be made, the elastic

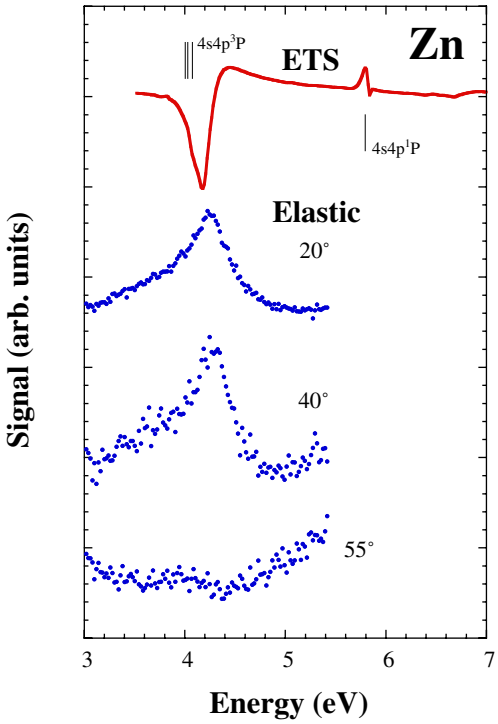

Figure 6. The derivative of the transmitted electron current (top), and the differential elastic scattering signal for zinc as a function of energy in the vicinity of the 4s4p excited state thresholds. For the elastic scattering data the zeros of each spectrum have been displaced.

scattering spectra also show the same overall trend as in Mg, particularly the absence of the strong resonance at an angle of 54°. Although we do not show it here due to the limited experimental data available for comparison, these general trends are also reproduced in the theoretical calculations.

4.3. Cadmium

The ETS spectrum for Cd is shown in figure 7 and, again, a wealth of resonance structures is observed below the ($^2S_{1/2}$) ionization potential at 8.99 eV. The positions of a number of the neutral excited states of Cd are also shown as vertical bars on the figure. With the increased spin–orbit splitting in Cd over that in Zn, more resonances are visible, e.g. in the region of the 5s5p ^{3}P thresholds. Once again, a strong feature coincides, within a few meV, with the energy of the 5s5p ^{1}P excited state and it has a width of 70−80 meV, similar to that observed in both Mg and Zn. Also, two broad features are observed well below the 5s6s ^{3}S threshold and one very broad resonance straddles the 5s6s ^{1}S threshold. At higher energies, the only significant difference between the spectra for Cd and Zn is that, surprisingly perhaps, there is only one resonance observed below (or at) the threshold of the 5s6p ^{3}P state, whereas in Zn two features were observed near the threshold of the 4s5p ^{3}P state. The ETS spectrum in the region of the 5s5p ^{3,1}P excited states is shown in figure 8 together with elastic scattering data at a number of scattering angles. Shown near the ETS spectrum are the positions of the

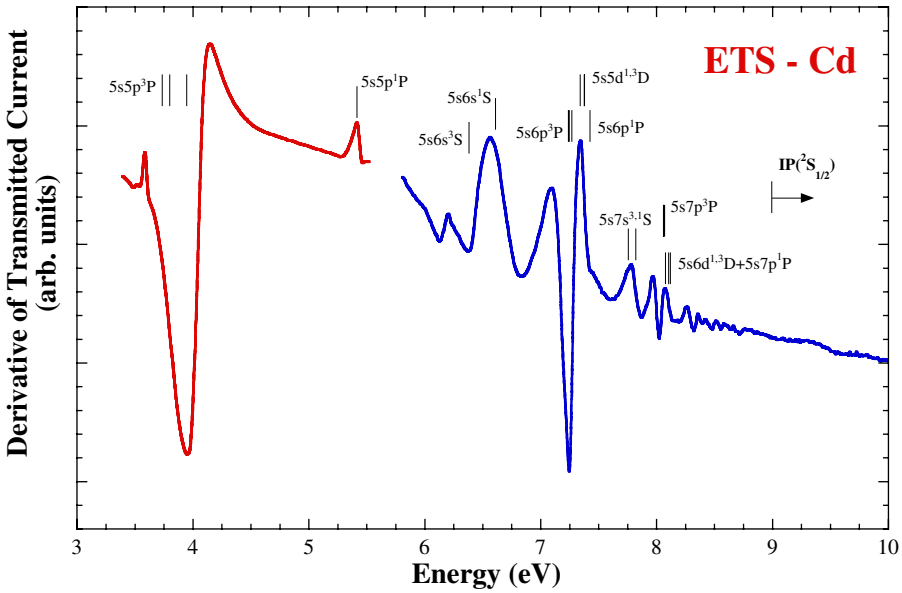

Figure 7. The derivative of the transmitted electron current for cadmium as a function of incident electron energy. The positions of a number of neutral excited states are indicated by the vertical bars.

$^3P_{0,1,2}$ and ^1P excited states and we can clearly see that the increased spin–orbit interaction in Cd has the effect of further separating the triplet excited states (energies of 3.734, 3.801 and 3.946 eV respectively), such that they are now resolvable by a spectrometer with conventional high resolution of ∼40 meV. We also see in the ETS spectrum, for the first time, the evidence of a *number* (at least two) of resonances at or near the ^3P thresholds, their visibility no doubt enhanced by the larger spin–orbit interaction and increased separation of their parent states. There is also evidence in the elastic scattering spectra in figure 8 (e.g. in the spectra for 120°) of additional resonances. Both the elastic scattering and ETS spectra show a further resonance at or near the threshold for the excitation of the 5s5p ^1P state. Interestingly, the elastic scattering spectra are very similar to those measured in magnesium and zinc.

In figure 9 we compare the elastic scattering measurements in the region of the 5s5p $^3P_{0,1,2}$ excited states with the results of the theoretical calculations, carried out with a 5-state Breit–Pauli approach. At each angle, the experiment has been normalized to the theory at an energy of 4 eV. As in the case of magnesium, the general features of the experiment are reproduced by the calculation and some of the differences which we see may be due to background scattering contributions in the experiment. At most of the angles, the calculation finds the main resonance feature at slightly higher energies than in the experiment, and in both the 24 and 120° spectra a number of weaker resonance features are observed below the main resonance, as in the experiment. At an angle of 90°, we once again see the elastic cross-section drop considerably as one passes through the 5s5p $^3P_{0,1,2}$ thresholds and at 54° there is almost a complete absence of any resonant scattering. At both 24 and 54° the calculated scattering cross-sections (direct plus resonant) are also extremely large.

Unlike the lighter Group II atoms, the significant spin–orbit interaction in cadmium leads to the 5s5p $^3P_1$ level being optically connected to the ground state with a substantial transition probability. In figure 10(a) we show the excitation function for the 5s5p $^3P_1 \rightarrow 5s^2\ ^1S_0$ transition

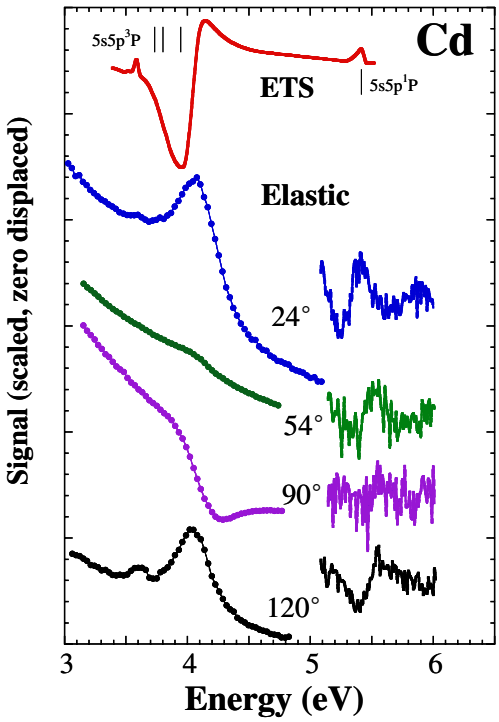

Figure 8. The derivative of the transmitted electron current (top), and the differential elastic scattering signal for cadmium as a function of energy in the vicinity of the 5s5p excited state thresholds. For the elastic scattering data the zeros of each spectrum have been displaced and above 4.8 eV a linear background has been subtracted from the spectrum to assist in highlighting the resonance features.

at 326.1 nm from threshold (3.801 eV) to about 9 eV. This cross-section is dominated by a strong, broad resonance, or series of resonances, within a few hundred meV above threshold. Several smaller features are observed at higher energies, in particular at or near the threshold for the $5s5p\,^1P_1$ state at 5.42 eV. We have indicated the position of a number of the neutral excited states of Cd with vertical bars and the higher-lying resonance features have been enhanced by background subtraction. In figure 10(b) we show the optical excitation function for the $5s5p\,^1P_1$ state, obtained by measuring the yield of 228.8 nm photons from the decay $5s5p\,^1P_1 \rightarrow 5s^2\,^1S_0$. As in the case of Mg, this cross-section rises rather slowly from threshold with only a few weak resonance features evident. There is, however, a relatively sharp step in the cross-section at threshold. Several resonances are observed near the thresholds of higher-lying excited states and once again these have been enhanced in the lower panel by background subtraction.

Also shown in each frame of figure 10 is a comparison of these optical excitation functions with the RM calculations. In figure 10(a) for the ^3P state, the experimental peak height has been normalized to that of the theory and, while there is overall agreement between the shape of the two cross-sections, the theoretical curve peaks at a higher energy and is substantially broader than that observed experimentally. The agreement between experiment and theory for the excitation function of the ^1P state (figure 10(b)) is relatively good (experiment has been

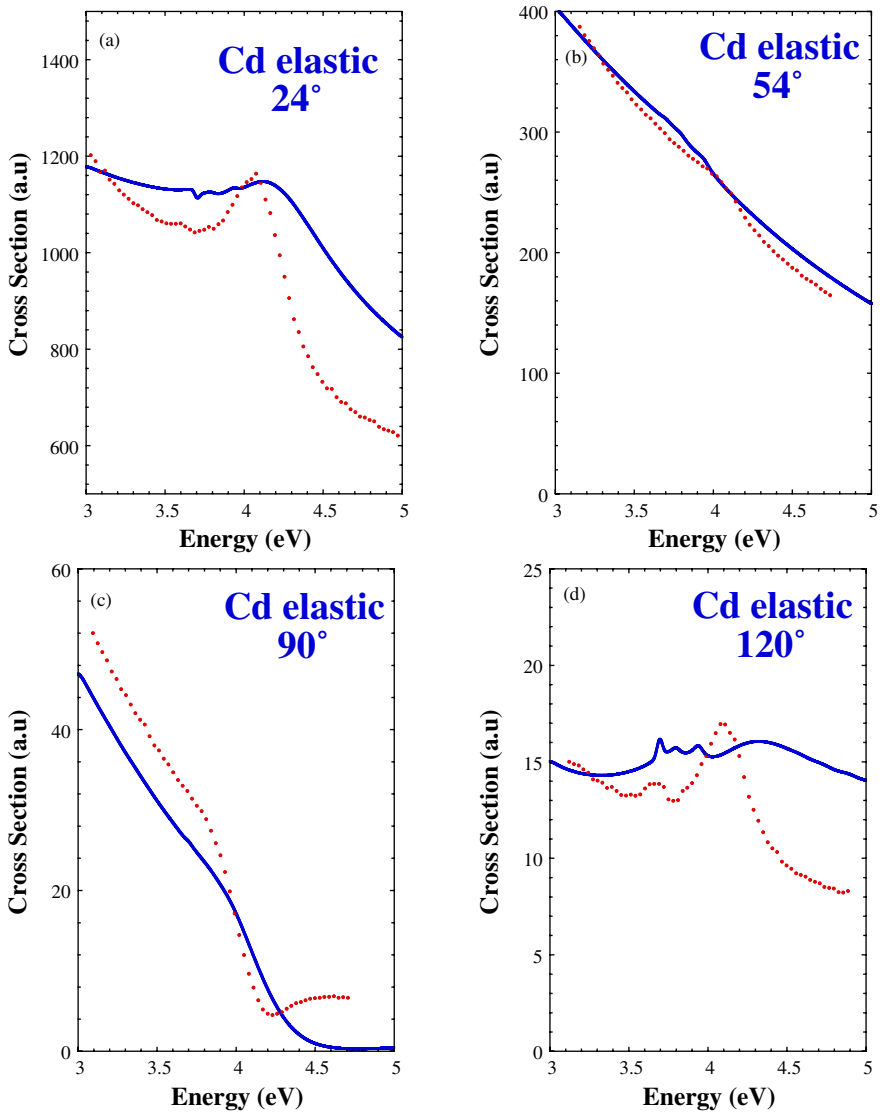

Figure 9. Comparison of experiment and predictions from a 5-state Breit–Pauli RM calculation (solid line) for elastic electron scattering from Cd at (a) 24°, (b) 54°, (c) 90° and (d) 120°. In each case the experimental results have been normalized to theoretical results at an energy of 4 eV. The vertical scale is in atomic units (a.u.).

normalized to theory at 7 eV) and the theory also predicts the sharp threshold feature which is seen in the experimental result.

The above results for cadmium can be compared, to some extent, with the recent measurements of Kontros *et al* [13]. The important thrust of their work appears to have been the determination of absolute cross-sections, with their energy resolution of 150 meV enabling only the more prominent resonance features to be observed. In their total cross-section there is clear evidence for a broad resonance near the threshold for the $5s5p\,^3P_{0,1,2}$ states. Also, their total, averaged cross-section for the excitation of the $5s5p\,^3P_{0,1,2}$ states is similar in shape

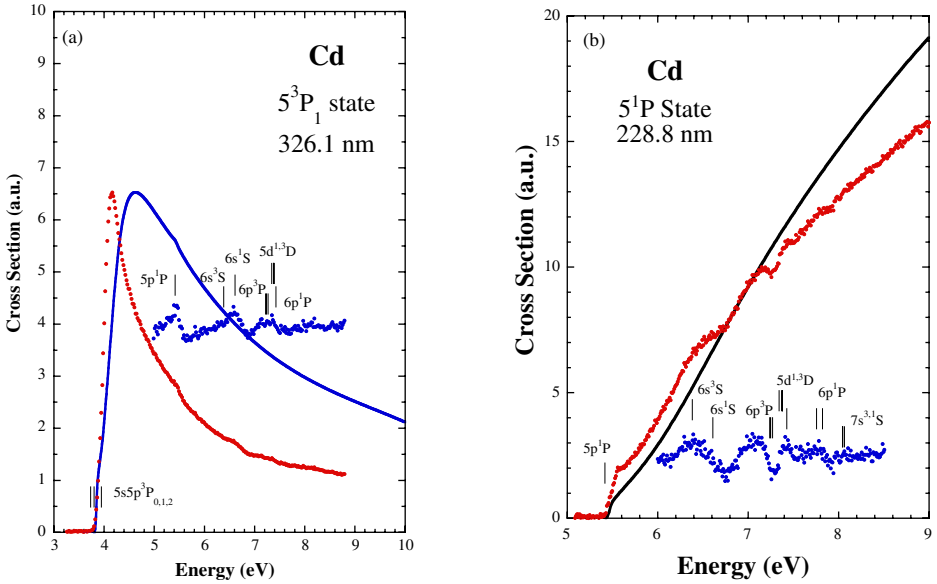

Figure 10. Optical excitation function for the (a) $5s5p\,^3P$ and (b) $5s5p\,^1P$ states of cadmium between threshold and 10 eV. In each case, the solid line is the 5-state Breit–Pauli RM calculation to which the experimental data have been normalized. In (a) the experimental results have been normalized to the peak height of the theoretical results while in (b) they have been normalized at an energy of 6 eV. The vertical bars indicate the energies of excited state thresholds, some of which are labelled. The vertical scale is in atomic units (a.u.). In both figures the small resonance features at higher energies have been highlighted by subtracting a smoothly varying background.

to the present measurement of the $5s5p\,^3P_1$ state shown in figure 10(a) with a strong and broad threshold resonance evident. There is also good general agreement between the present measurement (figure 10(b)) and that of Kontros *et al* for both the shape and magnitude of the excitation cross-section for the $5s5p\,^1P$ state, including the sharp onset near threshold.

4.4. Mercury

Mercury has been studied much more extensively than any of the Group IIA or B atoms. In many respects it also provides the best vehicle for the study of resonances in the Group II atoms as it has the largest spin–orbit interaction, and thus the largest energy splitting of states within individual excited manifolds. Also, the total energy span of the singly excited states in Hg is larger than the other atoms (~5.76 eV from the $6s6p\,^3P_0$ state at 4.67 eV to the $^2S_{1/2}$ ionization potential at 10.43 eV) and, as these excited states form the parent states for the resonances under study, the resonances are thus more widely spread in Hg than in any other Group IIB atom.

The ETS spectrum for Hg is shown in figure 11 and once again we see evidence for a large number of negative ion resonances. Also shown in this figure are the locations of some

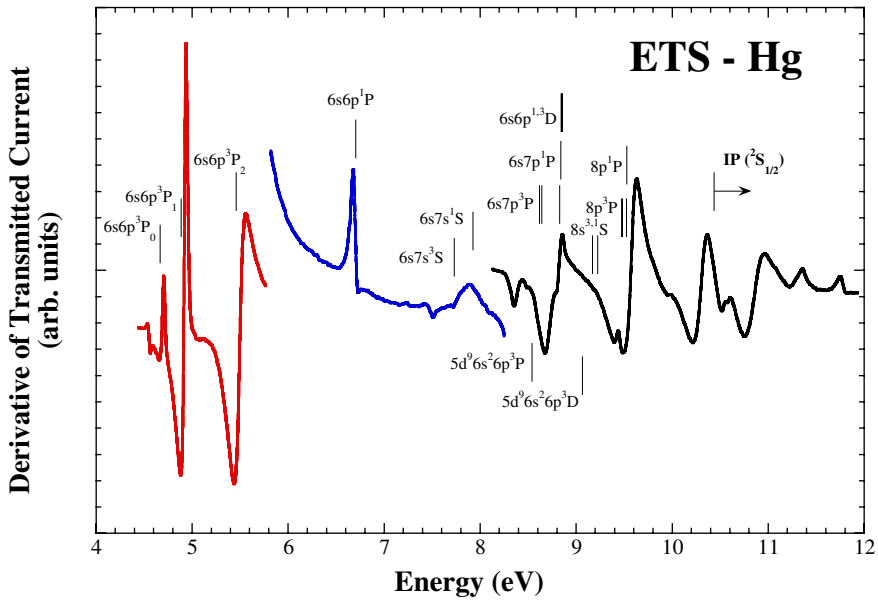

Figure 11. The derivative of the transmitted electron current for mercury as a function of incident electron energy. The positions of a number of neutral excited states are indicated by the vertical bars.

of the neutral excited states of Hg. In particular, we can see that the 6s6p ^{3}P manifold of states is now clearly separated, as are a larger number of resonance features located in the vicinity of these states. In all, four distinct resonances can be identified in the ETS spectrum in this energy region, whilst at the 6s6p ^{1}P threshold, another strong feature is observed. Note also that this latter resonance is considerably narrower than similar features observed near the corresponding ^{1}P threshold for the lighter Group II atoms. Once again two resonances are observed in the energy region between the 6s6p ^{1}P and 6s7s ^{3}S states, although their appearance in the Hg ETS spectrum is somewhat different from that for the lighter atoms. There is also a small feature which occurs very close in energy to the 6s7s ^{3}S threshold. Another significant difference in the Hg spectrum is the appearance of a resonance at about 8.35 eV, between the 6s7s ^{1}S and 6s7p ^{3}P thresholds. A similar feature is not observed in the lighter atoms. At higher energies, the Hg ETS spectrum is substantially different from those of the lighter atoms and this is due to the presence of core excited states with configurations $5d^9 6s^2 6p$. These issues are discussed further in the next section. Amongst the higher-lying features is a series (or multiple series) which extends above the ionization potential, converging presumably on the higher-lying ionization limits of 14.84 eV ($^2D_{5/2}$) and 16.705 eV ($^2D_{3/2}$).

In figure 12 we show the details of the ETS spectrum in the vicinity of the 6s6p ^{3,1}P states as well as measurements of elastic backscattering. In a previous communication [21] we have demonstrated how a phase-shift analysis of these spectra, and the measurements of electron spin-polarization by Albert *et al* [17], provide strong evidence for the existence of five resonances in the energy region of the ^{3}P thresholds. These results are discussed in the next section.

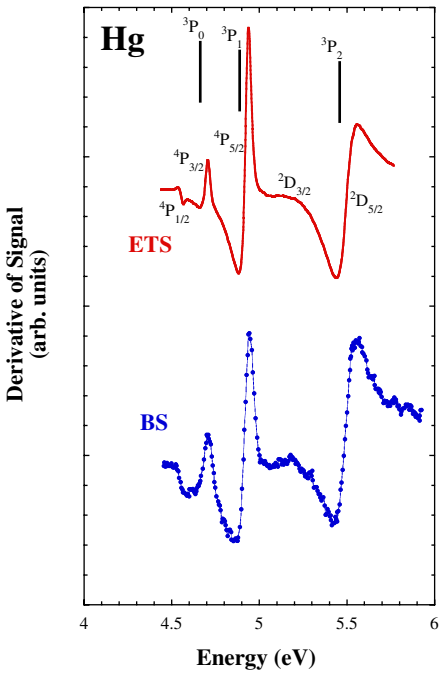

Figure 12. The derivative of the transmitted electron current (top), and the backscattered signal for mercury as a function of energy in the vicinity of the 6s6p ^{3}P excited state thresholds. The zeros of each spectrum have been displaced.

5. Discussion and proposed resonance classifications

5.1. Region I

For the purposes of orderly discussion we shall divide the spectrum in each target atom into two regions, I and II. Region I rather loosely corresponds to the resonances associated with the $nsnp^2$ configurations in each atom ($n = 3, 4, 5, 6$ respectively for Mg, Zn, Cd and Hg). Region II extends from the upper end of Region I to the ionization potential.

5.1.1. Mercury. Given the comments that were made above regarding the use of mercury as the natural 'map' for studies of negative ion resonances in the Group II metals, we shall lead our discussion with a consideration of the spectra for Hg. This is particularly relevant for the resonances in the vicinity of the $nsnp\,^{3,1}P$ thresholds as most of the resonances that are observed in Hg in this energy region can be mapped onto the other Group II atoms, even though they may overlap strongly, or be degenerate, in the lighter species.

In the energy range of main interest to the present studies, the lowest-lying resonance configuration is expected to be $nsnp^2$ (where $n = 3, 4, 5, 6$ for Mg, Zn, Cd, and Hg respectively). Such a configuration can support a number of possible terms, $^2S_{1/2}$, $^2P_{1/2,3/2}$, $^2D_{3/2,5/2}$, and $^4P_{1/2,3/2,5/2}$ and, although most of these have been identified, there remain some outstanding questions. The question of the nature of the resonances in the region of the 6s6p ^{3}P excited states has largely been resolved in previous work. The most recent of this is a precursor of the present study [20] where we drew on a number of experimental approaches, including the ETS and BS data shown in figure 12, but also a range of previous studies such as

Table 1. Energies and proposed classifications of resonance features in Region I for Hg

Feature energy (eV)	Feature width (meV)	Proposed configuration
4.550	0.46	$6s6p^2\ ^4P_{1/2}$
4.670	14.7	$6s6p^2\ ^4P_{3/2}$
4.915	∼60	$6s6p^2\ ^4P_{5/2}$
5.12	∼290	$6s6p^2\ ^2D_{3/2}$
5.53	∼280	$6s6p^2\ ^2D_{5/2}$
6.70	∼20	$6s6p^2\ ^2S_{1/2}$

the differential elastic scattering and spin-polarization studies of Duweke *et al* [32] and Albert *et al* [17] and the metastable atom excitation functions of Koch *et al* [18] and Newman *et al* [19]. Burrow *et al* [21] used a phase-shift analysis of the various published measurements to support the existence of five resonances in the region of the $6s6p\ ^3P$ states, namely the $^4P_{1/2}$, $^4P_{3/2}$, $^4P_{5/2}$, $^2D_{3/2}$ and $^2D_{5/2}$ states. The main thrust of this work was the additional evidence for the broad and weak $^2D_{3/2}$ resonance, at an energy of 5.15 eV, which had been the topic of some discussion since the earliest measurements (see e.g. [15, 16]). As was discussed in detail by Bartschat and Burke [33] the significant splitting of the $^2D_{3/2}$ and $^2D_{5/2}$ states indicates a strong configuration interaction effect. In a non-relativistic single-configuration description, these states would be exactly degenerate—independent of the strength of the spin–orbit interaction. Thus, of the eight resonances which we might expect to see associated with the $6s6p^2$ configuration in Hg, five lying in the vicinity of the $6s6p\ ^3P$ states are now believed to be reliably classified and these are summarized in table 1. The energies and widths of these states are updated in this table to reflect what we believe are the best contemporary estimates but we stress that they draw heavily on many of the previous measurements and assessments (see [21] for details).

The identification and classification of the remaining three resonance terms ($^2S_{1/2}$, $^2P_{1/2}$, $^2P_{3/2}$) for the $6s6p^2$ configuration has proven somewhat more elusive. In the metastable excitation function measurements of Newman *et al* [19] they assign a strong, narrow feature at an energy of 6.702 eV, very close to the $6s6p\ ^1P$ threshold at 6.704 eV, to the $6s6p^2\ ^2S_{1/2}$ resonance. A similarly strong feature is observed in the ETS spectrum (figure 10) at an energy of 6.69 eV. As we have seen, similar features are observed at the corresponding threshold in the other Group II atoms but, in the case of Hg, the resonance appears to be considerably narrower—the higher resolution measurements of Newman *et al* indicate a width of about 20 meV (FWHM). Unfortunately, there are no angular distribution measurements in this energy region in Hg to assist the classification of this state. Presumably, measurements in the elastic channel, for instance, would be able to confirm the presence of this state in the incident and scattered $s_{1/2}$ wave. However, such measurements in the present work for Cd, e.g. figure 8, do appear to support this hypothesis. Thus we conclude that the feature near 6.7 eV is most likely the $6s6p^2\ ^2S_{1/2}$ resonance. Alternatively, it may be a cusp structure associated with the opening of a new channel. The latter viewpoint is consistent with the fact that numerical calculations of the relevant partial waves over a very fine energy mesh could not detect any further substantial structure in the partial-wave cross-sections, which could be assigned, e.g. to the $^2P_{1/2}$, and $^2P_{3/2}$ states. The assignment of a cusp is also more consistent with the shape of the feature that is observed in the ETS spectrum.

Newman *et al* [19] further classified two broad features between 6.3−6.8 and 7.6−8.1 eV as the remaining terms of the $6s6p^2$ configuration, namely $^2P_{1/2}$ and $^2P_{3/2}$, respectively. These classifications were based on considerations of isoelectronic sequences, angular momentum and parity conservation and predictions of the 'modified Rydberg formula' [24]. They too are yet to be tested by an experiment where the angular momentum of the scattered electron can be determined unambiguously. In the ETS spectra (figure 11) there is no evidence for the lower-energy feature although, given its strength and width in the metastable spectrum, this is perhaps not surprising. In the energy region (7.6–8.1 eV) of the upper of the two weak features identified by Newman *et al*, a number of structures are observed in the ETS data below, and overlapping, the thresholds for the $6s7s\ ^{1,3}S$ excited states. These include a weak and narrow dip in the spectrum at 7.73 eV, coinciding with the threshold of the $6s7s\ ^3S$ excited state, and a broad peak, centred at 7.89 eV, about 35 meV below the threshold for the $6s7s\ ^1S$ excited state. The features in the ETS spectrum are more pronounced and apparently narrower than those in the metastable spectrum and they are also duplicated in the spectra for Mg, Zn and Cd. We believe that they are most likely associated with configurations above $6s6p^2$ and this will be discussed later.

Also in this region, at an energy of 7.48 eV in the ETS spectrum, there is another resonance structure which is about 300 meV below the threshold for the $6s7s\ ^3S$ state. This feature was also observed by Newman *et al* in their metastable atom excitation function at an energy of 7.50 eV and tentatively classified by them as $6s7s^2\ ^2S_{1/2}$. Once again we shall leave a detailed discussion of this to the next section.

5.1.2. Cadmium. We may expect to find some significant differences in the ETS spectrum for Cd (figure 7) compared with that for Hg in the region of the $5s5p\ ^3P$ excited states due to the reduced spin–orbit splitting of the energy levels in the former. As a result, the different J components of the ^4P and ^2D manifolds will be spaced by smaller amounts and the ^4P multiplet may be reduced in magnitude because of the smaller entrance width. In particular, the lowest-lying $^4P_{1/2}$ component, which has a width of ∼0.5 meV in Hg, may be even narrower and weaker in Cd. Also, as the background phase shifts for Cd [34] in this energy region are similar to those for Hg, we might expect the resulting resonance profiles to be similar to Hg.

In figure 7 we see that the first two resonance features in this region of the Cd spectrum lie significantly below the energy of the $5s5p\ ^3P_0$ state, unlike in Hg where they are close to, or overlap, the energies of the neutral excited states. Given the discussion above regarding the $^4P_{1/2}$ state we classify these, at 3.50 and 3.56 eV respectively, as the $5s5p^2\ ^4P_{3/2,5/2}$ states. The broad, dominant feature in the spectrum at 4.05 eV is attributed to the $^2D_{3/2,5/2}$ states which are not resolved. The elastic scattering spectra, and theoretical calculations in figures 8 and 9, provide further support for these classifications. The $5s5p^2$ configuration is of even parity and each of the $^4P_{3/2,5/2}$ and $^2D_{3/2,5/2}$ terms would be expected to decay to the even parity $5s^2\ ^1S_0$ ground state by the autodetachment of a d-wave electron. Although the two lowest-lying features are not resolved in the elastic spectrum, the reduced intensity of all of the resonance features near the ^3P thresholds in the 54° spectrum is consistent with the proposed classifications.

The excitation function (EF) for the decay photons from the $5s5p\ ^3P$ state, shown in figure 10(a), is dominated above threshold (3.734 eV) by a strong resonance. This feature,

Table 2. Energies and proposed classifications of resonance features in Region I for Mg, Zn and Cd

	Resonance energy (eV)		
Proposed configuration	Magnesium ($n = 3$)	Zinc ($n = 4$)	Cadmium ($n = 5$)
$nsnp^2\,{}^4P_{1/2}$	–	3.82	–
$nsnp^2\,{}^4P_{3/2}$	–	3.82	3.50
$nsnp^2\,{}^4P_{5/2}$	–	3.82	3.56
$nsnp^2\,{}^2D_{3/2}$	∼2.8	4.25	4.05
$nsnp^2\,{}^2D_{5/2}$	∼2.8	4.25	4.05
$nsnp^2\,{}^2S_{1/2}$ (?)	4.32	5.79	5.41

which results in a peak in the EF at an energy of 4.15 eV, is almost certainly due to the $^2D_{3/2,5/2}$ states and the dominant contribution is most likely from the $^2D_{3/2}$ state as this can decay to the odd parity $^3P_0$ level by the autodetachment of a p-wave electron, whereas the $^2D_{5/2}$ state requires an outgoing f-wave electron to conserve parity and angular momentum.

The next prominent feature in the ETS spectrum of Cd (figure 7) is a resonance at 5.41 eV, which lies just a few meV below the 5s5p ^1P threshold (5.417 eV). It is also seen in the optical EF for the 5s5p $^3P_0$ state, and although it appears to overlap the threshold in this spectrum, the statistical quality of the data is not such that a definitive energy can be determined. Interestingly, the optical EF for the 5s5p ^1P state (figure 10(b)) shows a sharp step at threshold which is consistent with a threshold resonance. Although the proximity of this resonance to the ^1P threshold is similar to what is observed in Hg, the width of this resonance, from the ETS data, appears to be much larger (∼50 meV). By analogy with Hg and the classification of Newman *et al*, this feature would be due to the $^2S_{1/2}$ term of the $5s5p^2$ resonance configuration. The resonance is also observed in the differential elastic scattering data (figure 8) and the angular distribution is consistent with such a classification, as it would decay to the elastic channel via an autodetached s-wave electron.

At higher energies we see a feature which lies well below the 5s6s ^3S state and another below the ^1S threshold. These will be discussed later. The energies and classifications for the Cd resonances in Region I are summarized in table 2.

5.1.3. Zinc. Once again the trend to smaller spin–orbit splitting is continued in Zn and, as a result, we see only two resonance features in the ETS spectrum near the 4s4p ^3P thresholds in figure 5. The first and weakest of these, barely discernible in the ETS spectrum, lies at about 3.82 eV, 200 meV below the $^3P_0$ level. This feature is most likely due to the $4s4p^2\,{}^4P_{1/2,3/2,5/2}$ resonances. The second and dominant feature at about 4.25 eV is broadly classified as ^2D as no splitting is observed. Once again the (somewhat more limited) elastic scattering data, shown in figure 5, supports this classification.

The next prominent feature in the Zn spectrum occurs at 5.79 eV, again within a few meV of the 4s4p ^1P threshold which is located at 5.797 eV. Once again the width of this feature is about 60 meV. There are no further data either in elastic scattering or optical excitation functions with which to compare in the case of Zn.

At higher energies we again see similar features as were observed in Hg and Cd below, in the case of Zn, the 4s5s $^{3,1}S$ thresholds. An additional feature, which does not appear to have

an analogue in either Hg or Cd, is observed at about 6.2 eV, some 450 meV below the $5s\,^3S$ threshold. These features are discussed in a later section. The energies and classifications for the Zn resonances in Region I are summarized in table 2.

5.1.4. Magnesium. In addition to being the lightest of the Group II elements that we consider here, magnesium also has the smallest spin–orbit splitting and differs significantly from the other elements in that it does not have any d-shell electrons. In the region of the $3s3p\,^3P$ states (whose threshold energies are 2.709, 2.712 and 2.717 eV, i.e. separated by only 8 meV), only one large resonance is observed and, in line with the trend we have followed from mercury to zinc, we classify this feature as the $3s3p^2\,^2D$ resonance—the ^4P state remains essentially invisible since it can only couple to the entrance channel through non-conservation of the total spin, quite an unlikely process for such a light target as Mg. This is supported by the elastic scattering spectra and the theoretical calculation, shown at various scattering angles in figures 2 and 4. In particular, we note that the absence of the resonance in the spectrum at 54° is entirely consistent with this classification.

The next resonance that we observe is at an energy of 4.32 eV, about 20 meV below the threshold for the $3s3p\,^1P$ state. This energy is in contrast to the corresponding feature in each of the other atoms studied, where the resonance was within a few meV of the threshold. This feature is also observed in the elastic scattering data of figure 2 where it appears that the contribution to the cross-section of the resonance vanishes at 90°. The one caveat that we would place on this observation is that the elastic scattering cross-section at 90° drops precipitously (almost to zero) at energies above the ^2D feature and the statistical quality of the data is marginal. This observation, which is consistent with the resonance decaying by the autodetachment of a p-wave electron, is in contrast to that in Cd, for instance, where the elastic scattering angular distribution was consistent with an outgoing s-wave electron for the corresponding feature. The width of this feature in both the ETS and optical data also appears to be in excess of 100 meV which continues the trend of the increasing width observed for Hg, Cd and Zn. In Hg this feature was classified by Newman *et al* as the $^2S_{1/2}$ term of the $6s6p^2$ configuration. This is also a likely candidate in Mg, although it is possible that there are also contributions from the other expected terms of the $3s3p^2$ configuration, namely $^2P_{1/2,3/2}$. Finally, we note that while the excitation function for the $3s3p\,^1P$ state (figure 3) is essentially featureless, there is some evidence of a step at threshold, similar to the corresponding EF in Cd.

Two further features are observed in the vicinity of the $3s4s\,^{3,1}S$ thresholds in both the ETS and photon data. These are discussed in the following section. The energies and classifications for the Mg resonances in Region I are summarized in table 2.

5.2. Region II

In the higher reaches of the negative ion spectra of these atoms it transpires that the ETS spectra for Zn and Cd are remarkably similar and, perhaps even more surprisingly, are also quite similar to that of Mg. Hg, on the other hand, is entirely different in this energy region and this is due, no doubt, to the presence of core-excited states with configurations $5d^96snl$ that lie below the first ionization threshold.

A further remarkable feature of the ETS spectra is the degree to which the resonance structure duplicates itself at successively higher n levels in a given atom. This has prompted

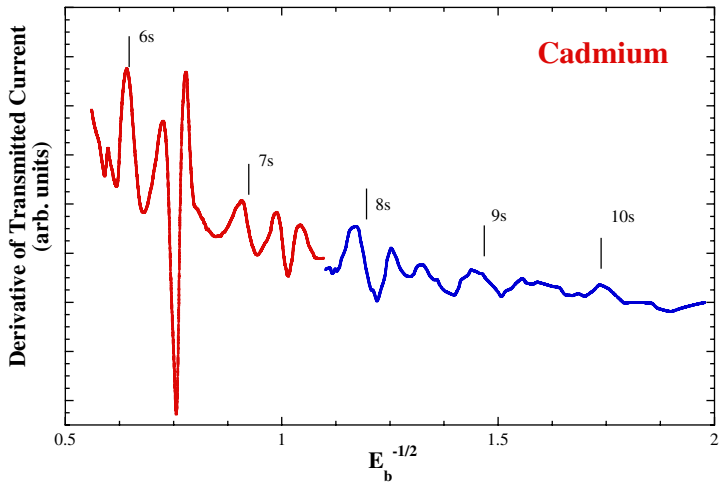

Figure 13. The derivative of the transmitted electron current for cadmium as a function of $E_b^{-1/2}$ where E_b has been defined in the text. The positions of a number of neutral excited states are indicated by the vertical bars.

us to consider a novel way of presenting the data that draws on the observed regularities to hopefully simplify the classification of the features by concentrating on the lowest group of resonances in one atom and then extrapolating these findings to the higher n levels. In addition, this technique has also been useful in identifying those resonances in Hg that are associated with the $5d^{10}6snl$ excited states.

The process we have used to help in the identification of higher energy resonances involves the use of a non-linear energy scale. If we assume, for simplicity, that quantum defects are negligible it is well known that the binding energies of excited atomic Rydberg states with respect to the ionization potential are given by

$$E_b = R/n^2.$$

Thus the energy spacing between adjacent levels goes to zero as the ionization potential is approached. In the present case, we wish to spread the states such that the separations are equal for any n level. That is, we wish to plot the data on a scale in which n is uniformly spaced. From the above equation

$$n = R^{1/2} E_b^{-1/2}$$

and, plotting the ETS data versus $E_b^{-1/2}$ should enable us to achieve the desired result.

We begin by illustrating the similarity of the resonance structures for successively higher n levels in Cd, which is chosen since the quality of the higher energy data was the best of the series. Figure 13 shows the derivative of the transmitted current in Cd as a function of the binding energy, with respect to the lowest ionization potential (the $^2S_{1/2}$ at 8.994 eV). To guide the eye we also include a series of vertical bars which are placed at the energies of the $ns\,^1S$ states for $n = 6$–10, as indicated. Note that each vertical bar lies just above a peak in the spectrum and that the spacing between each of these peaks and the nearby bar changes marginally with n because of the non-zero quantum defects. As n increases, the

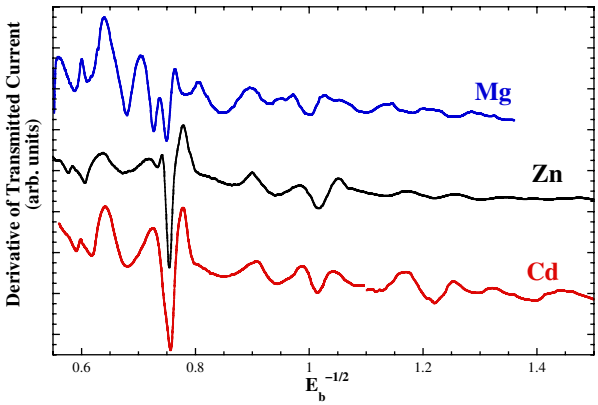

Figure 14. The derivative of the transmitted electron current for magnesium, zinc and cadmium as a function of $E_b^{-1/2}$.

instrumental energy resolution becomes insufficient to resolve the resonances. Nevertheless, figure 13 shows the remarkable similarity in the resonance structures for successive n levels with each exhibiting three major positive extrema and one negative, at least up to $n = 8$.

The next step in examining the regularities in the resonance spectra of the lighter Group II atoms is to compare, in the same fashion, the spectra for Mg, Zn and Cd and this is done in figure 14. Note that as we have used the binding energy from the first ionization potential of each atom (7.644 eV for Mg, 9.391 eV for Zn, 8.994 eV for Cd) the horizontal axis is the same for all. It can be seen that the spectra for Zn and Cd are almost identical with respect to the position of the major structures and once again the structures are repeated at successively higher values of n. In the Mg spectrum the second and third family of features also displays the same repetition and is also quite similar to the spectra for Zn and Cd although there appears to be a drift in the energy of the features to lower values.

For the corresponding energy region in Hg, the resonances have been extensively studied in the metastable excitation function of Newman *et al* and the majority of the features that they observed have been assigned to resonances associated with $5d^9 6s^2 nl$ core-excited parent states. By plotting the Hg spectra in a similar fashion, using the binding energy of the $5d^{10}6s$ state of Hg^+ (10.43 eV), and comparing it with the Cd spectrum, it should then be possible to identify those features which are associated with core-excited resonances. This is done in figure 15. For values of $E_b^{-1/2}$ below about 0.75 the two spectra are very similar, suggesting that assignments of the features will be common to both atoms. The pronounced dip just above 0.75 and the peaks on either side of it are also common. However, in the case of Hg, there is a second peak on the high energy side, at about 8.85 eV, i.e. for $E_b^{-1/2} \sim 0.80$, which is just above the threshold for the $5d^9 6s^2 6p\ ^3D$ metastable state. The correspondence of the lower feature with the feature in Cd indicates that it probably belongs to a $5d^{10}6snl$ parent state while the upper one, identified by Newman *et al* as feature 'L', is probably a core excited state. With the possible exception of a feature at $E_b^{-1/2} \sim 1.0$ (~9.43 eV, feature 'M' in the work of Newman *et al*), this plot also indicates that the upper reaches of the ETS spectrum for Hg are probably dominated by core-excited resonances.

Using these plots, and those shown earlier on a linear scale, together with the extensive investigation of Newman *et al*, tentative assignments of some of the resonance features can be offered. At $E_b^{-1/2} \sim 0.6$ in figure 14, the feature common to the spectra of all four metals,

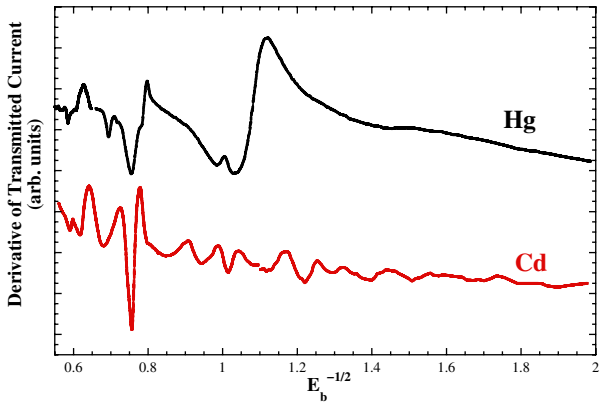

Figure 15. The derivative of the transmitted electron current for mercury and cadmium as a function of $E_b^{-1/2}$.

and lying just below the $ns(n+1)s\,^3S$ threshold, is most likely the $ns(n+1)s^2$ resonance. This feature is located at ~4.85 eV in Mg, ~6.4 eV in Zn, ~6.15 eV in Cd and ~7.48 eV in Hg ($n = 3, 4, 5, 6$ respectively). This classification is also aided by the similar classification for the Hg feature in the work of Newman *et al*, where it occurs at an energy of 7.50 eV in the metastable excitation function. The next feature in each spectrum is a broad resonance lying between the $ns(n+1)s\,^3S$ and ^1S neutral excited states (at an energy of ~5.25 eV in Mg, 6.75 eV in Zn and ~6.5 eV in Cd) and we tentatively assign this to the $ns(n+1)s(n+1)p$ configuration. The next feature in the spectra of Mg and Zn, and perhaps Cd, at $E_b^{-1/2} \sim 0.7$ is also quite broad and may be due to the configuration $ns(n+1)snd$. This occurs at ~5.6 eV in Mg and ~7.4 eV in Zn. The position and indeed, the existence, of the corresponding feature in Cd is, at best, uncertain. In Hg, however, there is a pronounced feature at this value of $E_b^{-1/2}$ (see figure 15), corresponding to an energy of ~8.30 eV. A feature at this energy in the metastable atom excitation function has been classified by Newman *et al* as the onset of the core excited neutral state $5d^96s^26p$, although they provide no discussion on this choice. It is unlikely that the feature in the ETS spectrum could be due to such a threshold so this resonance could either be a configuration similar to those observed in Mg and Zn at this value of $E_b^{-1/2}$, that is 6s7s6d, or it may be the lowest lying member of the $5d^96s^26p^2$ configuration. Given the apparent absence of the $ns(n+1)snd$ configuration in Cd, we favour the latter, very tentative, classification. The next strong feature in each spectrum (including Hg) occurs at $E_b^{-1/2} \sim 0.76$. This is near the threshold for the $ns(n+1)p\,^3P$ neutral excited state and, by analogy with the spectra in the region of the $nsnp\,^3P$ threshold, this is probably the $ns(n+1)p^2\,^2D$ resonance. It occurs at ~5.9 eV in Mg, ~7.65 eV in Zn, ~7.25 eV in Cd and ~8.7 eV in Hg. Finally, in both Mg and Zn there is a further weak but relatively narrow feature at $E_b^{-1/2} \sim 0.73$ (~5.77 and ~7.55 eV respectively) which may be due to the configuration $nsnd^2$. The energies and tentative classifications for these resonances in Mg, Zn, Cd and Hg in region II are summarized in table 3. It is also relevant to note that a number of these states described above are observed in the optical excitation functions for Cd, shown in figure 10.

Although it is clear that there are many more features observed in the higher energy reaches of the ETS spectra for each of these atoms, and it may be possible to extrapolate some of the above classifications to higher values of n, any attempt would be highly speculative and we refrain from attempting such.

Table 3. Energies and proposed classifications of resonance features in Region II for Mg, Zn, Cd and Hg

	Resonance energy (eV)			
Proposed configuration	Magnesium ($n = 3$)	Zinc ($n = 4$)	Cadmium ($n = 5$)	Mercury ($n = 6$)
$ns(n+1)s^2$	4.85	6.4	6.15	7.48
$ns(n+1)s(n+1)p$	5.25	6.75	6.5	
$ns(n+1)snd$	5.6	7.4	–	
$nsnd^2$	5.77	7.55	–	
$(n-1)d^9ns^2np^2$	–	–	–	8.3
$ns(n+1)p^2\,{}^2D$	5.9	7.65	7.25	8.7

6. Conclusions

We have presented new experimental and theoretical evidence for resonances in the two-electron systems Mg, Zn, Cd and Hg. The experimental investigations cover measurements of electron transmission spectra, optical excitation functions and differential elastic scattering. Each of these techniques offers new and complementary information on both the energies and tentative classifications for the large number of temporary negative ion states (resonances) that are observed. The experimental work is supported by new theoretical calculations, based on the RM technique, which show excellent agreement with the experimental results and assist in the classification of the lower-lying resonances. They also serve the extremely important function of providing an absolute scale for the normalization of some of the experimental results. While the present work provides, for the first time, tentative classifications for many of the resonant states, further measurements involving the differential (in angle) detection of scattered electrons would be useful for unravelling the higher reaches of the spectra of each atom. The Hg atom could be a good target for such measurements at incident energies above ~6 eV.

Acknowledgments

This work was supported by the Australian National University and by the United States National Science Foundation (KB and PB). Most of the calculations were performed during a visit of KB to the Australian National University, which was supported through an International Researcher Exchange (IREX) grant from the Australian Research Council.

References

[1] Buckman S J and Clark C W 1994 *Rev. Mod. Phys.* **66** 539
[2] Burrow P D, Michejda J A and Comer J 1976 *J. Phys. B: At. Mol. Phys.* **9** 3225
[3] Burrow P D and Comer J 1975 *J. Phys. B: At. Mol. Phys.* **8** L92
[4] Johnston A R and Burrow P D 1982 *J. Phys. B: At. Mol. Phys.* **15** L745
[5] Andersen T, Andersen H H, Balling P, Kristensen P and Petrunin V V 1997 *J. Phys. B: At. Mol. Phys.* **30** 3317
[6] Pegg D J, Thompson J S, Compton R N and Alton G D 1987 *Phys. Rev. Lett.* **59** 2267

[7] Walter C W and Peterson J R 1992 *Phys. Rev. Lett.* **68** 2281
[8] Shpenik O B, Zapesochnyi I P, Kontrosh E E, Nepiipov E I, Romanyuk N I and Sovter V V 1979 *Sov. Phys. – JETP* **49** 426
[9] Shpenik O B, Zapesochnyi I P, Sovter V V, Kontrosh E E and Zavilopulo A N 1973 *Zh. Eksp. Teor. Fiz.* **65** 1797
[10] Zapesochnyi I P, Sovter V V, Shpenik O B and Zavilopulo A N 1974 *Dokl. Akad. Nauk. SSSR* **214** 1288
[11] Bartsch M, Geesmann H, Hanne G F and Kessler J 1992 *J. Phys. B: At. Mol. Opt. Phys.* **25** 1511
[12] Panajotovic R, Minic M, Marinkovic B, Pejcev V and Filipovic D 1994 *17th Summer School and Int. Symp. on the Physics of Ionised Gases (SPIG 17), Belgrade 1994* Contributed papers, p 16
[13] Kontros J E, Szoter L, Chernyshova I V and Shpenik O B 2002 *J. Phys. B: At. Mol. Phys.* **35** 2195
[14] Kontros J E, Chernyshova I V and Shpenik O B 2003 *Tech. Phys.* **48** 964
[15] Heddle D W O 1975 *J. Phys. B: At. Mol. Phys.* **8** L33
[16] Heddle D W O 1978 *J. Phys. B: At. Mol. Phys.* **11** L711
[17] Albert K, Christian C, Heindorff T, Reichert E and Schön S 1977 *J. Phys. B: At. Mol. Phys.* **10** 3733
[18] Koch L, Heindorff T and Reichert E 1984 *Z. Phys.* A **316** 127
[19] Newman D S, Zubek M and King G C 1985 *J. Phys. B: At. Mol. Phys.* **18** 985
[20] Hanne G F, Nickich V and Sohn M 1985 *J. Phys. B: At. Mol. Phys.* **18** 2037
[21] Burrow P D, Michejda J A, Lun D R, Sullivan J P, McEachran R P, Newman D S and Buckman S J 1998 *J. Phys. B: At. Mol. Phys.* **31** L1009
[22] Buckman S J *et al* 1999 *Aust. J. Phys.* **52** 473
[23] Sanche L and Schulz G J 1972 *Phys. Rev.* A **5** 1672
[24] Rohr K 1977 *J. Phys. B: At. Mol. Phys.* **10** 2215
[25] Moore C E 1971 *Atomic Energy Levels (National Standards Reference Data System)* (Washington, DC: US Govt Printing Office)
[26] Scott N S, Burke P G and Bartschat K 1983 *J. Phys. B: At. Mol. Phys.* **16** L361
[27] Eissner W, Jones M and Nussbaumer H 1974 *Comput. Phys. Commun.* **8** 270
[28] Hibbert A 1975 *Comput. Phys. Commun.* **9** 141
[29] Berrington K A, Eissner W B and Norrington P H 1995 *Comput. Phys. Commun.* **92** 290
[30] Burke V M and Noble C J 1995 *Comput. Phys. Commun.* **85** 471
[31] Herting C, Hanne G F, Bartschat K, Grum-Grzhimailo A N, Muktava K, Srivastava R and Stauffer A D 2002 *J. Phys. B: At. Mol. Phys.* **35** 4439
[32] Duweke M, Kirchner N, Reichert E and Staudt E 1973 *J. Phys. B: At. Mol. Phys.* **6** L208
[33] Bartschat K and Burke P G 1986 *J. Phys. B: At. Mol. Phys.* **19** 1231
[34] McEachran R P and Stauffer A D 1992 *J. Phys. B: At. Mol. Phys.* **25** 1527